BIOCHEMISTRY
including biophysical chemistry & molecular biology

Article

pubs.acs.org/biochemistry

Thermodynamics and Kinetics of Adaptive Binding in the Malachite Green RNA Aptamer

Jason B. Da Costa, Aurelia I. Andreiev, and Thorsten Dieckmann*

Department of Chemistry, University of Waterloo, 200 University Ave West, Waterloo, ON N2L3G1, Canada

Supporting Information

ABSTRACT: Adaptive binding, the ability of molecules to fold themselves around the structure of a ligand and thereby incorporating it into their three-dimensional fold, is a key feature of most RNA aptamers. The malachite green aptamer (MGA) has been shown to bind several closely related triphenyl dyes with planar and nonplanar structures in this manner. Competitive binding studies using isothermal titration calorimetry and stopped flow kinetics have been conducted with the aim of understanding the adaptive nature of RNA−ligand interaction. The results of these studies reveal that binding of one ligand can reduce the ability of the aptamer pocket to adapt to another ligand, even if this second ligand has a significantly higher affinity to the free aptamer. A similar effect is observed in the presence of Mg^{2+} ions which stabilize the binding pocket in a more ligand bound-like conformation.

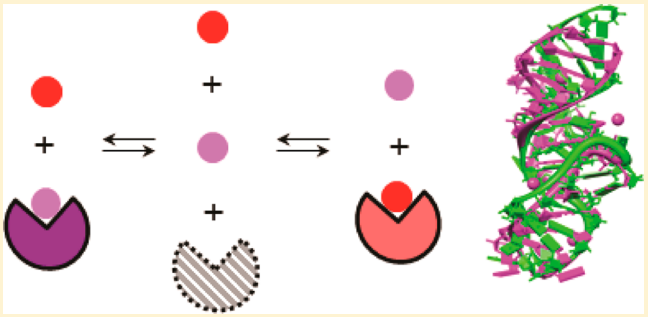

Aptamers are short nucleotide sequences that bind to their targets with high affinity and specificity.[1,2] RNA aptamers have been developed using systematic evolution of ligands by exponential enrichment (SELEX) for a variety of targets.[3,4] The malachite green RNA aptamer (MGA) was selected to bind to malachite green (MG)[5,6] and delivers a clear spectroscopic signature upon binding.[6,7] It has been used in a variety of applications such as a binary probe for specific target sequences,[8] a chimeric probe for adenosine,[9] a diagnostic assay for MG,[10] and even in biomolecular computing.[11] MGA also constitutes an excellent model system to study RNA−small molecule interactions. We can use this model system to study the mode of binding found in most aptamers, the so-called adaptive binding or ligand induced folding.[12−16] A detailed understanding of these interactions is of significance for the development of RNA-based biosensors and for the use of RNA as a drug or drug target. This type of macromolecule−ligand interaction is characterized by a largely unstructured binding pocket in the RNA that adopts a well-defined structure only upon binding of the ligand, which frequently becomes an integral part of the three-dimensional structure.

Two structures of MGA have been determined to date: a crystal structure of the aptamer bound to tetramethylrosamine (TMR) and a solution NMR structure of the complex with MG.[5,17] These structures revealed that the interaction between MGA and its ligand lacks hydrogen bonding and relies solely on stacking and electrostatic interactions. This provided the opportunity to study the capacity of RNA to interact with small molecules in the absence of hydrogen bonding. These studies led to the discovery of an intrinsic catalytic capability in the MGA. An ester derivative of MG undergoes an RNA catalyzed hydrolysis reaction when binding to MGA.

The reaction within the RNA binding pocket proceeds via a proton driven pathway, while the free MG ester hydrolysis proceeds via an OH-driven pathway.[18] The ability of MGA to catalyze a chemical reaction was not part of selection pressure applied during the SELEX procedure and illustrates the ability of RNA to incorporate multiple functions within the same molecule. More recently, it was shown that MGA changes its preference from the original ligand MG to TMR in the presence of Mg^{2+}.[19] This observation emphasizes the environment dependent character of RNA-ligand interactions. The MGA binding pocket consists of a base quadruple (C7, G24, G29, A31) and a Watson−Crick base pair (G8, C28) with two base triples (C10, G23, A27 and U11, A22, A26) and a U turn motif providing the supporting framework.

A comparison of the two MGA structures in complex with MG and TMR (Figure 1) shows that the most significant difference lies in the stacking patterns of the RNA bases at the top and bottom of the pocket. The G8:C28 base pair and the upper part of the pocket are rotated in the MG complex relative to their position in the TMR complex (Figure 1C, bottom). This leads to an unstacking of G8 and ring A of the ligand, thereby making room for the nonplanar structure of MG. Another important element of the binding pockets is A30 (Figure 1 C top) which stacks with ring C of the ligand. A30 is part of a bulge/loop structure consisting of A30, A31, U32, and G33. In the crystal structure a Sr^{2+} ion (Figure 1B) is positioned to interact with the phosphate oxygen atoms of A30,

Received: May 1, 2013
Revised: August 7, 2013
Published: August 28, 2013

dx.doi.org/10.1021/bi400549s | *Biochemistry* 2013, 52, 6575−6583

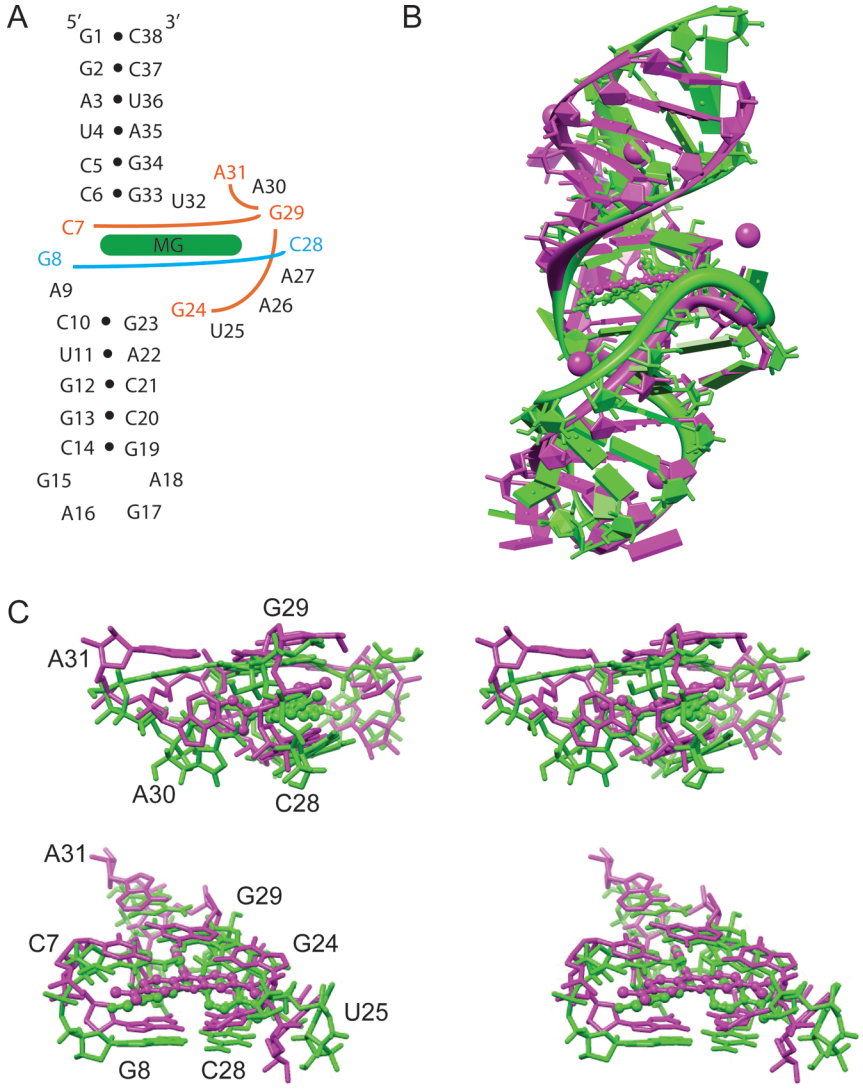

Figure 1. (A) Secondary structure schematic of MGA. The ligand MG is shown as green rounded box. Base-pairing interactions in the base quadruple and the G8:C28 base pair are indicated by orange and blue lines, respectively. (B) Superposition of the MGA NMR structure with bound MG (green, PDB ID 1Q8N) and the MGA crystal structure with bound TMR (purple, PDB ID 1F1T). The purple spheres indicate the position of Sr^{2+} ions in crystal structure. (C) Detailed view of the binding pocket of the superimposed structures in stereo view; top: back view; bottom: front view.

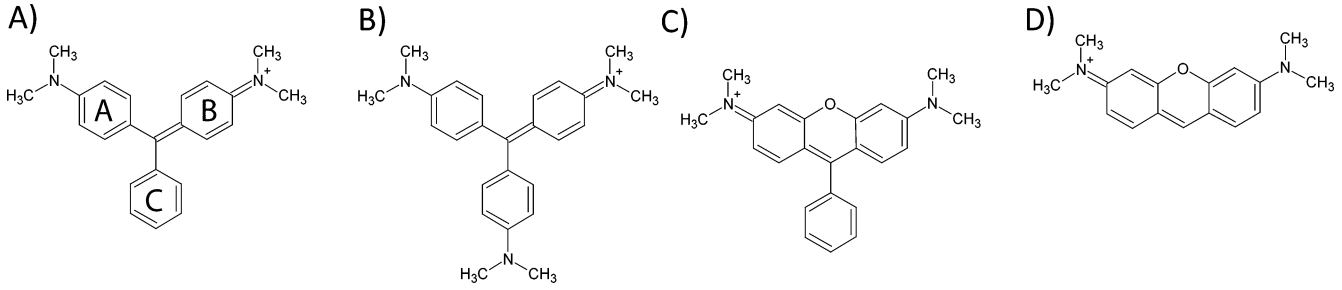

Figure 2. Chemical structures of dyes that bind to MGA (A) malachite green (MG), (B) crystal violet (CV), (C) tetramethylrosamine (TMR), and (D) pyronin Y (PY). The ring naming scheme used in the text is shown in structure A.

A31, and G33, whereas no divalent ions were present in the buffer used for the NMR studies.

Figure 2 shows the chemical structures of related dyes that bind to MGA. Pyronin Y (PY) has a planar structure similar to TMR but lacks the third ring, while crystal violet (CV) has a nonplanar structure similar to MG, with an extra dimethylamine group on ring C. Initial binding studies illustrated that the MGA binding pocket has the ability to adapt to recognize these related molecules.[5] This is consistent with the concept of adaptive binding. MG and TMR have higher affinities to MGA than CV and PY under all tested conditions. A comparison of our recent isothermal titration calorimetry (ITC) studies[19] with

dx.doi.org/10.1021/bi400549s | *Biochemistry* 2013, 52, 6575−6583

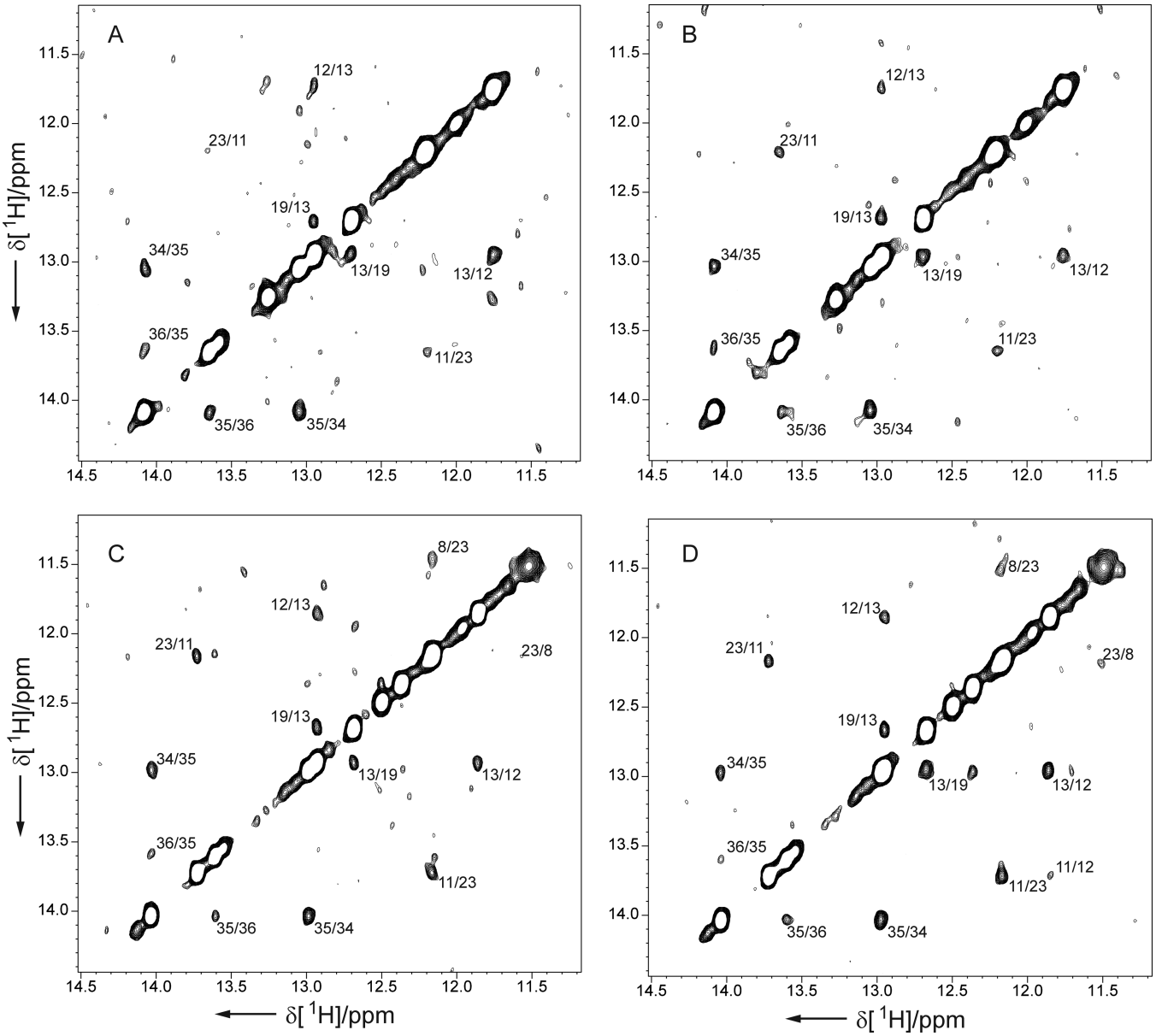

Figure 3. Imino proton regions of 2D 11-echo NOESY spectra of MGA at 283 K in 90% H_2O/10% D_2O (mixing time 150 ms). (A) Free MGA in 10 mM buffer. (B) Free MGA in 10 mM buffer and 10 mM Mg^{2+}. (C) MGA:TMR complex in 10 mM buffer. The Mg^{2+} was chelated with EDTA. (D) MGA:TMR complex in 10 mM buffer and 10 mM Mg^{2+}.

the earlier binding studies by Baugh et al. that used a competition binding assay[5] indicated that there might be differences in the way the free RNA and an aptamer with an already occupied binding site interact with a potential ligand. NMR experiments were conducted to better understand the free binding pocket under different buffer conditions. In order to further explore the changes that MGA undergoes when accommodating different ligands inside a free or occupied binding pocket, we have conducted competition binding experiments where PY or CV were prebound to MGA (MGA^{PY} and MGA^{CV}) while MG or TMR were titrated in. These thermodynamic studies were complemented with analogous stopped-flow kinetics studies to characterize the rate of binding in the presence and absence of a previously bound ligand. These experiments illustrate how the aptamer adapts to a ligand when the binding pocket is already occupied by another small molecule.

EXPERIMENTAL PROCEDURES

Sample Preparation. The RNA used for ITC and NMR spectroscopy was prepared enzymatically from a synthetic DNA template (5′-TAATACGACTCACTATAGGATCCCGA-CTGGCGAGAGCCAGGTAACGAATGGATCC-3′) by using T7 RNA polymerase and unlabeled NTPs.[20,21] After transcription magnesium pyrophosphate was removed by centrifugation, and the RNA was collected by precipitation with ethanol. The RNA was then separated from NTPs and aborted transcription products by PAGE using a 12% gel. The RNA product was then extracted from the gel by electro-elution and run on a HiPrep 16/10 DEAE FF anion-exchange column (GE Healthcare, Uppsala, Sweden), followed by salt removal on a Hiprep 26/10 Desalting column (GE Healthcare, Uppsala, Sweden) and lyophilization to dryness. Prior to NMR, ITC, and stopped-flow experiments, the RNA was dissolved in the desired buffer and then heated to 368 K for 30 s followed by

dx.doi.org/10.1021/bi400549s | Biochemistry 2013, 52, 6575−6583

cooling on ice for 30 s and equilibration at room temperature for 5 min.

NMR samples for studying exchangeable protons were prepared by dissolving the lyophilized RNA in a 90% H_2O/10% D_2O solution. Samples used for studying nonexchangeable protons were prepared by dissolving the RNA in 99.996% D_2O (Cambridge Isotopes). All NMR samples were 500 μL in standard 5 mm NMR tubes with final RNA concentrations of 0.8 to 1.8 mM in 10 mM NaCl at pH 6.

Malachite green (≥96% purity, Sigma-Aldrich Corporation, Milwaukee, WI), tetramethylrosamine (≥97% purity, Invitrogen Corporation, Carlsbad, CA), pyronin Y (≥50% purity, Acros Organics, Geel, Belgium), and crystal violet (≥93% purity, Fisher Scientific Company, Ottawa, Ontario, Canada) were dissolved in water to make 20 mM stock solutions. Dye concentrations of stock solutions were verified by UV/vis spectrophotometry.

NMR Experiments. All spectra were collected on a Bruker DRX-600 spectrometer equipped with a HCN triple-resonance, triple-axis PFG probe. Solvent suppression for samples in 90% H_2O/10% D_2O was achieved using 1$\overline{1}$-spin echo pulse sequences[22] or WATERGATE.[23] Quadrature detection for the indirect dimensions in multidimensional experiments was achieved using the States-TPPI method.[24] Two-dimensional NOESY spectra[25] in 90% H_2O/10% D_2O were acquired at 283 K with a mixing time of 150 ms. In addition, a 2D CITY-TOCSY[26] with a mixing time of 50 ms, a DQF-COSY,[27] and NOESY spectra with mixing times of 250, 200, and 50 ms in 100% D_2O were measured at 293 K to facilitate resonance assignments. The spectra were analyzed and assigned as previously described.[17]

ITC Studies. Experiments were performed at 25 °C on a MicroCal ITC 200 microcalorimeter (MicroCal, Inc., Northampton, MA). The 10−15 μM RNA solution was prepared by dissolving lyophilized RNA in 10 mM sodium phosphate buffer, pH 6.7, at the desired salt concentration. The 100−150 μM dye solutions were prepared by dissolving solid dye in 10 mM sodium phosphate buffer, pH 6.7, at the desired salt concentration. RNA and dye for the preparation of prebound samples (MGA^{CV} or MGA^{PY}) were mixed in a 1:2 ratio. The ITC cell was filled with the prebound RNA solution and titrated with the second ligand (MG or TMR) solution from the syringe. Each experiment consisted of a single injection over 396 s at a continuous flow of 0.1 μL/s to a final molar ligand/RNA ratio of 1.5. Total runtime per injection was approximately 7 min. We chose the continuous injection method over the traditional stepwise injection in order to be able to complete the large number of necessary experiments in a reasonable time. All ITC experiments were performed in triplicate, and the standard deviation of these experiments is reported in the tables. In order to account for heat of dilution of dye solution, a blank run with the prebound dye buffered in cell and second dye in syringe was run and subtracted from the experimental run. Supporting Information Figure S1 shows examples of typical ITC raw data. The validity of the data obtained by continuous injection was verified by comparing the data obtained via the standard multiple injection method with a corresponding continuous injection set (Figure S2). No significant differences for binding constants or thermodynamic parameters were found. All data sets were analyzed and fitted using the Origin software package provided by MicroCal.

Kinetic Experiments. Stopped flow fluorescence experiments were performed using a Fluorolog 3-22 spectrofluorometer (HORIBA Jobin-Yvon Spec, Inc.) interfaced with SFM-4/Q (Molecular Kinetics, Inc.). All data were analyzed using BioKine 2.1 software (Molecular Kinetics, Inc.) and fit to a single exponential. All experiments were carried out in 10 mM phosphate buffer with 10 mM $MgCl_2$ at 298 K. Binding of TMR was measured at 584 nm with excitation at 270 nm. MG binding was measured at 656 nm with excitation at 600 nm. PY binding was measured at 566 with excitation at 270 nm. CV binding was measured at 646 nm with excitation at 600 nm. The experiments were carried out at a constant RNA concentration of 1.5 μM with a dye concentration of 6 μM. For competition binding kinetics the RNA was mixed with CV at a 2:1 dye:RNA ratio before starting experiment. The acquisition of data was set to 5000 pts at 20 μs/pt followed by 2000 pts at 100 μs/pt and 1000 pts at 500 μs/pt. The measurements were performed in triplicate.

RESULTS AND DISCUSSION

Characterization of Free RNA by NMR Spectroscopy. One of the key features of adaptive binding in RNA aptamers is the absence of detectable structure in the ligand-free RNA binding pocket. In order to establish if this applies to MGA, we analyzed the base pairing patterns present in the aptamer RNA in absence of the ligand by high-resolution NMR spectroscopy (Figure 3).

Four 2D NOESY spectra were acquired in H_2O in order to observe structural changes associated with the presence of ligand and Mg^{2+}. The imino proton region of the first NOESY spectrum (Figure 3A), which contained only MGA in low salt buffer, showed evidence for the formation of the two stem structures on either side of the binding pocket. No indication of the formation of the binding pocket can be seen beyond the G12:U11 base pair in stem II and the C5:G33 base pair in stem I. Upon addition of 10 mM $MgCl_2$ (Figure 3B) an imino−imino NOE associated with a G23:U11 interaction appears, indicating the stabilization of the G23:C10 base pair. However, no evidence for the formation of the base triples or any of the base pairs in the binding pocket can be found. The two NOESY spectra at the bottom are acquired in the presence of a small excess of TMR in low salt buffer (Figure 3C) and with 10 mM Mg^{2+} (Figure 3D). In these spectra the formation of the binding pocket can be seen by the presence of the G23−G8 interaction which indicates the stacking of the G8:C28 base pair on the C10:G23:A27 base triple. In addition, there are numerous NOEs between RNA and ligand (data not shown).

The analysis of the NOE data indicates that the aptamer does not have a preferred stable structure for most nucleotides in the internal loop in the absence of a ligand. However, there is evidence for the formation of the G23:C10 base pair at the top of stem II in the presence of Mg^{2+}. This base pair forms a base-triple with A27 in the ligand bound aptamer and provides a base for the binding pocket by stabilizing the loop that forms its back side (U25, A27, and A26). However, there is no indication that the base triple is formed in the absence of ligand. The structures of the MGA−MG and MGA−TMR complexes (Figure 1) show that the binding pocket adopts a somewhat different structure when binding MG (a nonplanar ligand) versus TMR (a ligand with planar rings A + B). It was previously observed that the presence of divalent ions, such as Mg^{2+}, affects the association between MGA and its ligands. More specifically, when Mg^{2+} is present, the aptamer shows a larger increase in affinity for TMR than for MG, its original ligand (ΔK_d(TMR) = 0.98 ± 0.08 μM vs ΔK_d(MG) = 0.70 ±

dx.doi.org/10.1021/bi400549s | Biochemistry 2013, 52, 6575−6583

Table 1. ITC Determined Thermodynamic Parameters for MG and TMR Binding to MGA_{PY} or MGA_{CV} Complexes at Different Salt Concentrations, pH 6.7 at 25 °C, Using the Displacement Model

salt concn	prebound	titrant	n	K_d (μM)	ΔH (kcal mol^{-1})	ΔS (cal mol^{-1} K^{-1})	ΔG (kcal mol^{-1})
150 mM NaCl	CV	MG	0.52 ± 0.01	0.10 ± 0.01	−91.6 ± 0.43	−276 ± 1.53	−9.37 ± 0.07
	PY	MG	0.52 ± 0.12	0.50 ± 0.16	−37.1 ± 0.71	−95.5 ± 1.61	−8.65 ± 0.23
	CV	TMR	n/a	n/a	n/a	n/a	n/a
	PY	TMR	0.61 ± 0.02	0.32 ± 0.07	−21.8 ± 0.46	−43.4 ± 1.94	−8.86 ± 0.12
1 mM NaCl, 10 mM $MgCl_2$	CV	MG	0.54 ± 0.05	0.13 ± 0.02	−60.6 ± 0.53	−171 ± 1.79	−9.40 ± 0.09
	PY	MG	0.74 ± 0.06	0.21 ± 0.06	−28.8 ± 1.84	−66.0 ± 6.72	−9.11 ± 0.16
	CV	TMR	n/a	n/a	n/a	n/a	n/a
	PY	TMR	1.39 ± 0.58	0.27 ± 0.07	−19.5 ± 1.66	−34.6 ± 5.81	−9.25 ± 0.26

Table 2. ITC Determined Thermodynamic Parameters for MG and TMR Binding to MGA^{PY} or MGA^{CV} Complexes at Two Different Salt Concentrations, pH 6.7 at 25 °C, Based on the Single Site Model

salt concn	prebound	row no.	n	titrant	K_d (μM)	ΔH (kcal mol^{-1})	ΔS (cal mol^{-1} K^{-1})	ΔG (kcal mol^{-1})
150 mM NaCl		1	0.28 ± 0.06	CV	4.45 ± 0.08	−78.3 ± 14.6	−238 ± 49.1	−7.35 ± 0.09
		2	1.07 ± 0.02	PY	4.08 ± 0.20	−17.8 ± 0.38	−35.0 ± 1.20	−7.37 ± 0.03
		3	0.84 ± 0.08	MG	0.28 ± 0.06	−25.9 ± 2.24	−56.9 ± 8.54	−8.98 ± 0.14
	CV	4	0.52 ± 0.01	MG	1.40 ± 0.15	−14.3 ± 0.46	−21.1 ± 1.63	−7.97 ± 0.07
	PY	5	0.40 ± 0.23	MG	1.92 ± 0.42	−20.7 ± 1.07	−43.1 ± 3.87	−7.82 ± 0.13
		6	1.27 ± 0.10	TMR	0.28 ± 0.04	−18.3 ± 1.09	−31.4 ± 3.55	−8.95 ± 0.08
	CV	7	n/a	TMR	n/a	n/a	n/a	n/a
	PY	8	0.59 ± 0.02	TMR	2.72 ± 0.61	−4.62 ± 0.33	10.0 ± 1.49	−7.60 ± 0.12
1 mM NaCl, 10 mM $MgCl_2$		9	0.46 ± 0.07	CV	3.79 ± 0.12	−54.5 ± 9.71	−158 ± 32.60	−7.40 ± 0.01
		10	1.09 ± 0.07	PY	1.65 ± 0.67	−16.9 ± 1.77	−30.2 ± 6.52	−7.94 ± 0.23
		11	0.81 ± 0.11	MG	0.10 ± 0.01	−23.1 ± 1.35	−45.4 ± 4.42	−9.58 ± 0.04
	CV	12	0.53 ± 0.04	MG	0.81 ± 0.12	−6.61 ± 0.57	5.71 ± 1.75	−8.31 ± 0.09
	PY	13	0.72 ± 0.05	MG	1.01 ± 0.23	−12.5 ± 2.09	−14.5 ± 7.4	−8.19 ± 0.12
		14	1.36 ± 0.23	TMR	0.08 ± 0.02	−17.3 ± 1.51	−25.5 ± 5.26	−9.69 ± 0.12
	CV	15	n/a	TMR	n/a	n/a	n/a	n/a
	PY	16	1.29 ± 0.51	TMR	2.29 ± 0.88	−3.20 ± 1.44	15.2 ± 4.25	−7.73 ± 0.23

0.06 μM at 1 mM NaCl vs 1 mM NaCl/10 mM $MgCl_2$).[19] The crystal structure of the MG−TMR complex (Figure 1) which was obtained in the presence of Sr^{2+} shows that a divalent ion is bound near the G23:C11 base pair. It seems likely that this metal ion binding site is involved in stabilizing stem II in the presence of Mg^{2+} as evident from the NOESY spectra.

Competitive Isothermal Titration Experiments. The competition ITC studies were conducted at two different buffer conditions, 150 mM NaCl and 1 mM NaCl, 10 mM $MgCl_2$. These conditions are based on our previous ITC binding studies where we analyzed the binding interaction with free MGA.[19] The competition experiments were performed with PY or CV prebound to the aptamer since samples with prebound TMR and MG did not show any detectable signal when PY or CV as competing ligand were titrated in. This is expected since MG and TMR have significantly higher binding affinities than CV and PY.

As a first step, the binding affinities/complex dissociation constants for TMR and MG were measured using the displacement fitting approach from Sigurskjold.[28] Table 1 summarizes the binding data obtained from the competition experiments. The model used to fit the data has been previously shown to give the most accurate value for binding affinity of a ligand to the free receptor from competition ITC data. The model has been verified for multiple injections[28,29] and continuous injection.[30] The displacement binding model requires that the K_A and ΔH_A for binding of the prebound ligand (A) to the receptor (R) have been independently determined. The thermal power (P) generated upon titration of the second (competing) ligand (B) is then described by

$$P = \left(\left(\Delta H_A \frac{d([RA])}{dt}\right) + \left(\Delta H_B \frac{d([RB])}{dt}\right)\right)\left(V_0 \frac{dV}{dt} t\right) \quad (1)$$

where ΔH is the enthalpy change, V is the effective volume in the calorimeter cell, t is the time, and [RA] and [RB] are concentrations of receptor (R) bound to A or B.

With the known values for K_A and ΔH_A the values for K_B and ΔH_B can then be determined.[28−30] From Table 1 we see that the displacement model gives affinity values within experimental error to the ones obtained by our previous single ligand ITC experiments. TMR did not show any observable binding to the MGA^{CV} complex despite the fact that its affinity for free MGA is 16 times higher than that of CV. This can be explained by near perfect compensation of the heat of binding and dissociation involved in CV leaving the binding pocket and TMR binding.

The ΔH and ΔS values resulting from the displacement model (Table 1) are substantially different compared to those determined from binding to the free RNA.[19] The displacement binding model accounts for the heat of binding for the first ligand, and the thermodynamic variables determined by the fit are based on the assumption that the dissociation event involves the same energy amount as determined from the single ligand titration with the opposite sign. However, this is only completely correct if the aptamer returns after dissociation of the original ligand to the same structure or ensemble of conformations that was present in the free RNA. Thus, the

dx.doi.org/10.1021/bi400549s | Biochemistry 2013, 52, 6575−6583

observed differences of the thermodynamic parameters could be due to the different conformations and sampling of conformations space caused by the presence of a competing ligand. In order to better understand these differences, we analyzed the ITC data with the alternate single site model. This fit produced similar chi^2 values to the displacement model. Using this alternate model allows for direct comparison of the thermodynamic values to the results of binding to free RNA which were determined with the same model. The results of this analysis are summarized in Table 2.

Table 2 clearly illustrates the stabilizing effect of Mg^{2+}. The numbers in parentheses in the following discussion refer to the line numbers in Table 2. The ΔH and ΔS for MG binding to MGA in the presence (#3) and absence (#11) of Mg^{2+} are similar. However, the ΔH of binding to MGA^{CV} at 10 mM Mg^{2+} (#12) is only half that of the ΔH of binding in the absence of Mg^{2+} (#4). The reduced favorable ΔH is compensated by a decrease in unfavorable ΔS. The entropy change of adaptive binding in aptamers is generally unfavorable since the RNA pocket becomes highly structured upon binding. The smaller entropy penalty seen here could be the result of a preformed binding pocket. A similar change in ΔH and ΔS is seen in MG binding to MGA^{PY} in the presence (#13) and absence (#5) of Mg^{2+}. In both cases, the ΔH is less favorable by approximately 8 kcal mol^{-1} and the ΔS is more favorable by approximately 27 cal mol^{-1} K^{-1}. Interestingly, the change in buffers does little to change the ΔH and ΔS in the case of TMR binding MGA^{PY} (#8, 16). However, it is clear that TMR has a more favorable ΔS for binding to MGA^{PY} (#8, 16) than MGA (#6, 14) at both buffer conditions. While MG binding to MGA^{PY} (#5) has a similar ΔS compared to MG binding to MGA (#3), the ΔS for MG binding MGA^{CV} (#4) is more favorable than MG binding to MGA (#3). This suggests that MGA^{CV} has a binding pocket that slightly favors MG, while MGA^{PY} forms a pocket that facilitates binding of TMR.

This analysis shows that Mg^{2+} stabilizes the MGA binding pocket closer to its ligand binding conformation. The data also show that when MG replaces CV, there is a small entropy penalty compared to MG replacing PY. The absence of the third ring and the more planar structure in the case of PY would mean that the MGA pocket needs to undergo a conformational change to accommodate the third ring of MG. On the other hand, CV binding in the pocket involves interactions very similar to those of MG and hence does not require as many structural changes. TMR and PY differ only in the presence of the third ring, and thus only a small entropy increase is observed when TMR is replacing PY.

These results in combination with the NMR data illustrate that the presence of Mg^{2+} stabilizes the aptamer binding pocket in a conformation closer to its ligand bound structure. The presence of a prebound ligand has a similar effect in that it also preorganizes the aptamer binding pocket and thereby confers a smaller entropy penalty or small advantage. This is consistent with work by Sokolski et al., which has shown that the stability of free MGA affects binding by reducing the amount of RNA folded in the correct binding conformation.[31]

The n values for ligand binding to the free RNA have a similar trend to those reported by Sokoloski et al.,[31] with TMR binding to MGA having a much higher n value (1.40 ± 0.2) than MG binding to MGA (0.40 ± 0.02) (10 mM sodium cacodylate pH 5.8, 10 mM KCl and 10 mM $MgCl_2$). While the TMR binding n value is within error of our n value (1.36 ± 0.23) at 10 mM sodium phosphate pH 6.7, 1 mM NaCl and 10 mM $MgCl_2$, there is a significant difference in the n value for MG binding (0.81 ± 0.11); this could be due to the different conditions that allow the MGA pocket to explore more stable conformations. The Sokoloski et al. study[31] showed that the binding constants and n values were affected by temperature, injection time, and Mg^{2+} concentration. An increase in either temperature or injection time allows the aptamer to explore a larger conformational space resulting in a higher n value, while an increase in Mg^{2+} concentration leads to a decrease in n value due to the reduction of conformational space that is being explored.[31] The decrease of n value seen in the case of prebound ligands (see Table 1) suggests that MGA is restricted from exploring different conformations similar to the stabilizing effect of the bound metal ion. It should be mentioned that based on work by Tellinghusen[32] the K_d reported for CV and PY in our initial work may be less accurate due to the low c value used in the experiments. However, in this work we are comparing the effect of prebound CV and PY on the binding of MG and TMR, and hence the effect of this lower accuracy should be minimal.

Kinetic Binding Experiments. The kinetic studies were conducted at three different buffer conditions, 150 mM NaCl; 1 mM NaCl, 10 mM $MgCl_2$ and no added salt. In addition, experiments were also conducted with CV prebound to MGA at a 2:1 dye:RNA ratio. The MGA^{CV} complex was chosen for these studies because this complex offered a convenient observation of the binding kinetics via fluorescence. CV has no detectable fluorescence when not bound to the RNA, unlike PY which is fluorescent in both its free and RNA bound form. Table 3 summarizes the initial rates of binding from these experiments.

Table 3. Summary of Initial Binding Rates Determined from Stop Flow Experiments

RNA (1.5 μM)	salt concn	dye (6.0 μM)	rate [μM s^{-1}]
RNA	150 mM NaCl	TMR	50.44 ± 2.3
RNA	0	TMR	>150
RNA	10 mM $MgCl_2$	TMR	12.4 ± 0.32
2CV1RNA	10 mM $MgCl_2$	TMR	8.95 ± 0.25
RNA	150 mM NaCl	MG	29.14 ± 0.56
RNA	0	MG	58.75 ± 3.34
RNA	10 mM $MgCl_2$	MG	4.01 ± 0.08
2CV1RNA	10 mM $MgCl_2$	MG	2.84 ± 0.13
RNA	150 mM NaCl	PY	>150
RNA	0	PY	>150
RNA	10 mM $MgCl_2$	PY	41.8 ± 5.28
RNA	150 mM NaCl	CV	10.16 ± 0.84
RNA	0	CV	20.9 ± 2.1
RNA	10 mM $MgCl_2$	CV	2.71 ± 0.81

The results summarized in Table 3 show that TMR binds to MGA at a 1.7 times faster rate than MG in 150 mM NaCl solution. Binding for both TMR and MG is significantly slower in the presence of Mg^{2+} by a factor of 4 and 7.2 times, respectively. Together with the NMR and ITC results this illustrates that the increased stability of the preformed structure in the MGA binding pocket leads not only to a tighter binding but also to slower adaption to the ligand. The presence of a prebound ligand in the binding pocket has a similar effect; it also leads to a slowdown in initial binding rate by a factor of 1.4 for both TMR and MG. Interestingly, PY binding appears to be significantly faster and was only within the detectable limit

dx.doi.org/10.1021/bi400549s | Biochemistry 2013, 52, 6575−6583

when binding is slowed by presence of $MgCl_2$. The slow initial binding rate for MG and CV speaks to the amount of rearrangement needed to accommodate the larger, more flexible dyes. The slow kinetics of MGA binding also potentially contributes to the effect of injection time on the ITC data seen in the work reported by Sokoloski et al.[31]

CONCLUSIONS

In summary, the ITC and kinetic experiments described here show that MGA is kinetically trapped in a conformation or ensample of conformations that favors the first ligand it binds. This results in a reduced apparent affinity, even when challenged with a competing ligand that has a higher affinity for the free RNA than the prebound one. This becomes evident in a slower initial rate of binding in the presence of a competing ligand. The plasticity of the free RNA aptamer allows it to eventually adapt to somewhat differently shaped ligands, planar and nonplanar triphenyl dye derivatives in this case. Our ITC experiments and the analysis using two alternate binding models show that there is an energy penalty involved in restructuring the binding pocket. The kinetic work demonstrates that MG binds slower than TMR and the presence of magnesium reduces the initial rate of binding for both. On the basis of what we know about the effect of magnesium on thermodynamics and structure, we conclude that the penalty involved in restructuring the binding pocket is due to the RNA being kinetically trapped in a conformation that is not optimal for binding the new ligand. Mg^{2+} further stabilizes this conformation and thereby reduces the amount of conformational space that can be explored by the aptamer.

This observation can be explained by the ligand bound structure of the RNA representing an energy minimum in the RNA folding pathway. Hence, the molecule becomes trapped in the initially adopted conformation and requires additional energy and time to return to a partially unfolded state that can explore a larger conformational space and thus readily adapt to a differently shaped ligand. Fully characterizing this behavior is critical for understanding the way in which small molecules interact with RNA aptamers, for example, in biosensors where initial binding of a lower affinity ligand can potentially prevent detection of a high affinity target or in drug development where interactions between different potential ligands can reduce the efficiency of an RNA targeting drug in vivo.

The discussion of adaptive binding presented here focused on the thermodynamic and kinetic aspects of the binding process. From a structural point of view, there are two binding pathways that can be envisioned for adaptive binding in RNA aptamers. The first pathway assumes that the RNA binding pocket is structurally heterogeneous in solution, occupying many different conformations. The molecules with structures closest to the fully folded binding site recognize and bind the ligand. Because all conformations are in equilibrium with each other, this leads to more structures adopting a conformation suitable for binding until all ligand is bound or all RNA is in complex. The alternate pathway to adaptive binding assumes that the RNA binding pocket is largely unstructured in solution. When the ligand first interacts with the RNA via some recognition element, the RNA undergoes structural changes to form binding pocket in direct response to the presence of the ligand. The results presented here, as well as those recently published by Sokoloski et al.,[31] are in agreement with the first pathway to adaptive binding. However, a complex formation via the alternate pathway cannot be excluded at this time, and further studies of binding kinetics and thermodynamics will be necessary to clearly define the structural consequences of adaptive binding. A recent in-depth analysis of RNA binding pockets from many different structures by Kligun and Mandel-Gutfreund has shown that RNA binding pockets are rich in nucleotides with unique sugar puckers and nucleobase conformations. The authors propose that these conformations play a key role in RNA recognition by small molecule ligands and introduce the term "RNA conformational readout" for this process.[33]

The results presented here also explain the apparent contradiction between the binding affinities for MG (K_d = 800 nM at 10 mM Mg^{2+}) and CV (K_d > 1 mM at 10 mM Mg^{2+}) reported by Baugh et al.[5] and our recent ITC studies (K_d = 100 nM for MG and 3.8 μM for CV at 10 mM Mg^{2+}).[19] The earlier affinities were determined indirectly by measuring changes in TMR fluorescence anisotropy in competition experiments. The data presented here show that the required rearrangement of the binding pocket formation leads to an altered binding behavior if a ligand with a different structure is titrated in. The kinetic experiments revealed that the ligands have different binding rates when interacting with free or prebound aptamer. This indicates that determining the binding affinities of slow binders against a prebound fast binder by competitive fluorescence studies will underestimate the affinity of the slow binder when compared to the ITC studies. This possibility needs to be taken into account when designing experiments that characterize RNA aptamer–ligand interactions.

Kinetic studies of other aptamer–ligand systems have found mainly one step binding;[34−37] however, two-step binding processes have been revealed by studying variants of the thiamine pyrophosphate (TPP)[38] and 7-aminomethyl-7-deazaguanine aptamers.[39] A recent study using the novel kinITC approach, which obtains both kinetic and thermodynamic information from ITC experiments, has shown that the enthalpy term can be expressed as a combination of binding and folding terms using an analysis method that employs two distinct kinetic steps.[40] The application of this method to the TPP riboswitch confirmed that the switch is under kinetic control while the detection of TPP at the low cellular concentrations is thermodynamically driven.

ASSOCIATED CONTENT

Supporting Information

Figure S1: typical ITC raw data showing heat generated over time during representative continuous injection ITC experiments; Figure S2: comparison of ITC data showing heat generated over time during multiple and continuous injection ITC experiments; the multiple injection data have been integrated to allow for comparison; Figure S3: typical raw data obtained from a stopped flow fluorescence experiment, showing TMR binding to free MGA and TMR binding to MGA with CV prebound; Figure S4: native PAGE gel showing MGA and its complexes with MG and TMR; Figure S5: 1D NMR spectra corresponding to the 2D spectra shown in Figure 3. This material is available free of charge via the Internet at http://pubs.acs.org.

AUTHOR INFORMATION

Corresponding Author

*E-mail tdieckma@uwaterloo.ca; Fax +1-519-7460435; Tel +1-519-8884567 (T.D.).

Funding

This work was supported by the National Science and Engineering Research Council (NSERC) under grant no. 326911-2009 and the Canada Foundation for Innovation (CFI).

Notes

The authors declare no competing financial interest.

■ ACKNOWLEDGMENTS

Molecular graphics images were produced using the UCSF Chimera package from the Resource for Biocomputing, Visualization, and Informatics at the University of California, San Francisco.

■ ABBREVIATIONS USED

MGA, malachite green aptamer; MG, malachite green; SELEX, systematic evolution of ligands by exponential enrichment; TMR, tetramethylrosamine; PY, pyronin Y; CV, crystal violet; ITC, isothermal titration calorimeter; MGA^{PY}, PY prebound to MGA; MGA^{CV}, CV prebound to MGA.

■ REFERENCES

(1) Ellington, A. D., and Szostak, J. W. (1990) *In vitro* selection of RNA molecules that bind specific ligands. *Nature 346*, 818−822.

(2) Tuerk, C., and Gold, L. (1990) Systematic evolution of ligands by exponential enrichment: RNA ligands to bacteriophage T4 DNA polymerase. *Science 249*, 505−510.

(3) Carothers, J. M., Goler, J. A., Kapoor, Y., Lara, L., and Keasling, J. D. (2010) Selecting RNA aptamers for synthetic biology: investigating magnesium dependence and predicting binding affinity. *Nucleic Acids Res. 38*, 2736−2747.

(4) Proske, D., Blank, M., Buhmann, R., and Resch, A. (2005) Aptamers - basic research, drug development, and clinical applications. *Appl. Microbiol. Biotechnol. 69*, 367−374.

(5) Baugh, C., Grate, D., and Wilson, C. (2000) 2.8 angstrom crystal structure of the malachite green aptamer. *J. Mol. Biol. 301*, 117−128.

(6) Grate, D., and Wilson, C. (1999) Laser-mediated, site-specific inactivation of RNA transcripts. *Proc. Natl. Acad. Sci. U. S. A. 96*, 6131−6136.

(7) Nguyen, D. H., Dieckmann, T., Colvin, M. E., and Fink, W. H. (2004) Dynamics studies of a malachite Green-RNA complex revealing the origin of the red-shift and energetic contributions of stacking interactions. *J. Phys. Chem. B 108*, 1279−1286.

(8) Kolpashchikov, D. M. (2005) Binary malachite green aptamer for fluorescent detection of nucleic acids. *J. Am. Chem. Soc. 127*, 12442−12443.

(9) Xu, W. C., and Lu, Y. (2010) Label-free fluorescent aptamer sensor based on regulation of malachite green fluorescence. *Anal. Chem. 82*, 574−578.

(10) Stead, S. L., Ashwin, H., Johnston, B., Tarbin, J. A., Sharman, M., Kay, J., and Keely, B. J. (2010) An RNA-aptamer-based assay for the detection and analysis of malachite green and leucomalachite green residues in fish tissue. *Anal. Chem. 82*, 2652−2660.

(11) Hirabayashi, M., Ohashi, H., and Kubo, T. (2010) Design of bio-inspired multi-stage regulations for diagnostic molecular automata. *J. Comput. Theor. Nanosci. 7*, 831−839.

(12) Patel, D. J., Suri, A. K., Jiang, F., Jiang, L., Fan, P., Kumar, R. A., and Nonin, S. (1997) Structure, recognition and adaptive binding in RNA aptamer complexes. *J. Mol. Biol. 272*, 645−664.

(13) Gilbert, S. D., Reyes, F. E., Edwards, A. L., and Batey, R. T. (2009) Adaptive ligand binding by the purine riboswitch in the recognition of guanine and adenine analogs. *Structure 17*, 857−868.

(14) Hermann, T., and Patel, D. J. (2000) Biochemistry - adaptive recognition by nucleic acid aptamers. *Science 287*, 820−825.

(15) Dieckmann, T., Butcher, S. E., Sassanfar, M., Szostak, J. W., and Feigon, J. (1997) Mutant ATP-binding RNA aptamers reveal the structural basis for ligand binding. *J. Mol. Biol. 273*, 467−478.

(16) Dieckmann, T., Suzuki, E., Nakamura, G. K., and Feigon, J. (1996) Solution structure of an ATP-binding RNA aptamer reveals a novel fold. *RNA 2*, 628−640.

(17) Flinders, J., DeFina, S. C., Brackett, D. M., Baugh, C., Wilson, C., and Dieckmann, T. (2004) Recognition of planar and nonplanar ligands in the malachite green-RNA aptamer complex. *ChemBioChem 5*, 62−72.

(18) Brackett, D. M., and Dieckmann, T. (2006) Aptamer to ribozyme: the intrinsic catalytic potential of a small RNA. *ChemBioChem 7*, 839−843.

(19) Bernard Da Costa, J., and Dieckmann, T. (2011) Entropy and Mg^{2+} control ligand affinity and specificity in the malachite green binding RNA aptamer. *Mol. Biosyst. 7*, 2156−2163.

(20) Milligan, J. F., and Uhlenbeck, O. C. (1989) Synthesis of small RNAs using T7 RNA polymerase, in *Methods in Enzymology* (Dahlberg, J. E., and Abelson, J., Eds.), pp 51−62, Academic Press, New York.

(21) Milligan, J. F., Groebe, D. R., Witherell, G. W., and Uhlenbeck, O. C. (1987) Oligoribonucleotide synthesis using T7-RNA polymerase and synthetic DNA templates. *Nucleic Acids Res. 15*, 8783−8798.

(22) Sklenar, V., and Bax, A. (1987) Spin-echo water suppression for the generation of pure-phase two-dimensional NMR spectra. *J. Magn. Reson. 74*, 469−479.

(23) Piotto, M., Saudek, V., and Sklenar, V. (1992) Gradient-tailored excitation for single-quantum NMR spectroscopy of aqueous solutions. *J. Biomol. NMR 2*, 661−665.

(24) Marion, D., Driscoll, P. C., Kay, L. E., Wingfield, P. T., Bax, A., Gronenborn, A. M., and Clore, G. M. (1989) Overcoming the overlap problem in the assignment of ^{1}H NMR spectra of larger proteins by use of three-dimensional heteronuclear ^{1}H-^{15}N Hartmann-Hahn-multiple quantum coherence and nuclear Overhauser-multiple quantum coherence spectroscopy: application to Naturenterleukin 1β. *Biochemistry 28*, 6150−6156.

(25) Kumar, A., Ernst, R. R., and Wüthrich, K. (1980) A two-dimensional nuclear Overhauser enhancement (2D NOE) experiment for the elucidation of complete proton-proton cross-relaxation networks in biological macromolecules. *Biochem. Biophys. Res. Commun. 95*, 1−6.

(26) Briand, J., and Ernst, R. R. (1991) Computer-optimized homonuclear TOCSY experiments with suppression of cross relaxation. *Chem. Phys. Lett. 185*, 276−285.

(27) Piantini, U., Sørensen, O. W., and Ernst, R. R. (1982) Multiple quantum filters for elucidating NMR coupling networks. *J. Am. Chem. Soc. 104*, 6800−6801.

(28) Sigurskjold, B. W. (2000) Exact analysis of competition ligand binding by displacement isothermal titration calorimetry. *Anal. Biochem. 277*, 260−266.

(29) Wang, Z. X. (1995) An exact mathematical expression for describing competitive binding of two different ligands to a protein molecule. *FEBS Lett. 360*, 111−114.

(30) Markova, N., and Hallen, D. (2004) The development of a continuous isothermal titration calorimetric method for equilibrium studies. *Anal. Biochem. 331*, 77−88.

(31) Sokoloski, J. E., Dombrowski, S. E., and Bevilacqua, P. C. (2012) Thermodynamics of ligand binding to a heterogeneous RNA population in the malachite green aptamer. *Biochemistry 51*, 565−572.

(32) Tellinghuisen, J. (2008) Isothermal titration calorimetry at very low c. *Anal. Biochem. 373*, 395−397.

(33) Kligun, E., and Mandel-Gutfreund, Y. (2013) Conformational readout of RNA by small ligands. *RNA Biol.*, 10.

(34) Forster, U., Weigand, J. E., Trojanowski, P., Suess, B., and Wachtveitl, J. (2012) Conformational dynamics of the tetracycline-binding aptamer. *Nucleic Acids Res. 40*, 1807−1817.

(35) Lemay, J. F., Penedo, J. C., Tremblay, R., Lilley, D. M. J., and Lafontaine, D. A. (2006) Folding of the adenine riboswitch. *Chem. Biol. 13*, 857−868.

(36) Gilbert, S. D., Stoddard, C. D., Wise, S. J., and Batey, R. T. (2006) Thermodynamic and kinetic characterization of ligand binding to the purine riboswitch aptamer domain. *J. Mol. Biol. 363*, 624−624.
(37) Wickiser, J. K., Cheah, M. T., Breaker, R. R., and Crothers, D. M. (2005) The kinetics of ligand binding by an adenine-sensing riboswitch. *Biochemistry 44*, 13404−13414.
(38) Lang, K., Rieder, R., and Micura, R. (2007) Ligand-induced folding of the thiM TPP riboswitch investigated by a structure-based fluorescence spectroscopic approach. *Nucleic Acids Res. 35*, 5370−5378.
(39) Rieder, U., Kreutz, C., and Micura, R. (2010) Folding of a transcriptionally acting PreQ(1) riboswitch. *Proc. Natl. Acad. Sci. U. S. A. 107*, 10804−10809.
(40) Burnouf, D., Ennifar, E., Guedich, S., Puffer, B., Hoffmann, G., Bec, G., Disdier, F., Baltzinger, M., and Dumas, P. (2012) kinITC: A New Method for Obtaining Joint Thermodynamic and Kinetic Data by Isothermal Titration Calorimetry. *J. Am. Chem. Soc. 134*, 559−565.